N_2^+ first-negative emission cross sections for low-energy H^+ and H impact on N_2

B. Van Zyl, M. W. Gealy, and H. Neumann
Department of Physics, University of Denver, Denver, Colorado 80208
(Received 14 April 1983)

Absolute emission cross sections for the (0,1), (1,2), and (2,3) band emission sequence of the N_2^+ first-negative system have been measured for low-energy H^+ and H collisions with room-temperature N_2 molecules. The energy range covered for H^+ impact was from 63 eV to 2.0 keV, and that for H impact was from 160 eV to 2.5 keV. For $H+N_2$ collisions, cross sections for N_2 second-positive emissions for the (1,5) and (2,6) emission bands were also determined. The total cross sections for production of $N_2^+(B)$ and $N_2(C)$ were determined from these measured results. The techniques used to accomplish the measurements are described, and the cross sections obtained are compared with the results of other investigations.

I. INTRODUCTION

This paper reports measurements of the absolute cross sections for selected N_2^+ first-negative ($1N$) band emissions (belonging to the $B\,^2\Sigma_u^+ \rightarrow X\,^2\Sigma_g^+$ electronic transition) for low-energy proton (H^+) and hydrogen atom (H) impact on room-temperature N_2 molecules. The $1N(0,1)$, $1N(1,2)$, and $1N(2,3)$ emission bands were chosen for study because of their observationally convenient wavelengths (having heads at 427.8, 423.7, and 419.9 nm, respectively). Branching-ratio data presented here allow the emission cross sections for other bands originating from the $v'=0$, 1, and 2 vibrational levels of $N_2^+(B)$ to be determined from the measured results.

The goals of this study were threefold. First, because relatively few N_2^+ $1N$ band emission cross-section data were available for H^+ or H energies below 1 keV, it was felt useful to extend measurements of these important cross sections to lower projectile energies. The second goal was to investigate the amount of "unusual" vibrational excitation of $N_2^+(B)$ produced in the collisions (i.e., where the vibrational-level populations differ from those predicted by use of the Franck-Condon factors for the excitation process). The final goal was to place the measured results on a firm absolute basis. This was accomplished through a variety of comparisons between the photon signals measured during $H^+ + N_2$ and $H + N_2$ experiments with those measured during $e^- + N_2$ and $e^- + He$ experiments at 500-eV e^- energy, the latter signals resulting from processes with accurately known emission cross sections.

For $H + N_2$ collisions, the cross sections for the N_2 second-positive ($2P$) band emissions $2P(1,5)$ and $2P(2,6)$ were also determined. While these emissions (belonging to the $C\,^3\Pi_u \rightarrow B\,^3\Pi_g$ electronic transition) represented spectrally contaminating features in the N_2^+ $1N$ measurements, it was possible to computationally separate the photon signals from the two processes. Because the upper state for these emissions is $^3\Pi$, it is not readily populated by H^+ impact on N_2 in its ground $^1\Sigma$ state, the required electron spin flip being in violation of the Wigner spin-conservation rule. For H impact, this rule violation is bypassed via an electron exchange.

II. THEORY OF THE MEASUREMENTS

The basic technique used to measure the band emission cross sections was to prepare fast projectile beams of H^+, H, and e^- of known particle flux and energy and allow the projectiles to collide with N_2 in a target cell wherein the molecular density could be accurately determined. Photons resulting from the collisions were measured with a tilting-interference filter (TIF) fronting a cooled photomultiplier (henceforth called the TIF detector), which viewed the interaction region from a direction normal to the projectile-beam axes. By tilting the filter through an angular range from 0° to about 20°, wavelength scans over the spectral region containing the N_2^+ $1N$ emission band sequence of interest could be made.

For $e^- + N_2$ collisions, such wavelength-scan data were used in conjunction with theoretically simulated spectra of the rotational-line intensities within each of the N_2^+ $1N$ emission bands of interest to establish the properties of the TIF detector as a function of TIF angle. Supplementary information about properties of the TIF detector was obtained from wavelength scans over atomic-line emissions resulting from e^- collisions with He, Ar, and Kr. Comparisons of these wavelength-scan data with those obtained from $H^+ + N_2$ and $H + N_2$ collisions then allowed the desired band emission cross sections for these collisions to be determined relative to those for $e^- + N_2$ collisions. The remainder of this section is devoted to a discussion of the framework within which such comparisons could be made.

Consider a 300-K target cell containing low-density N_2 with number density N_{0k} molecules in their 0th vibrational level and kth rotational level. The projectile-beam flux moving parallel to the x axis through the cell is written as $I_b D(y,z)$. Here I_b is the total beam intensity and $D(y,z)$ is the spatial-distribution profile of the beam projectiles and satisfies $\int\int D(y,z)dy\,dz=1$. If the projectiles excite the N_2 to an upper electronic state in $0,k \rightarrow v',k'$ vibration-

rotation transitions, and the excited molecules decay to a lower electronic state in $v',k' \rightarrow v'',k''$ transitions giving photons of wavelength $\lambda_{v''k''}^{v'k'}$ the TIF detector when set at TIF angle θ will measure a photon signal given by

$$S_\theta(\lambda_{v''k''}^{v'k'}) = I_b \left[\sum_k N_{0k} \sigma_{0k}^{v'k'} \right] B_{v''k''}^{v'k'} E_\theta(\lambda_{v''k''}^{v'k'}) \ . \quad (1)$$

Here $\sigma_{0k}^{v'k'}$ is the excitation cross section for the $0,k \rightarrow v',k'$ transition, and $B_{v''k''}^{v'k'}$ is the branching ratio for the $v',k' \rightarrow v'',k''$ transition. $E_\theta(\lambda_{v''k''}^{v'k'})$ is an experimental parameter of the form

$$E_\theta(\lambda_{v''k''}^{v'k'}) = \int\int\int \epsilon_\theta(x,y,z,\lambda_{v''k''}^{v'k'}) \times \frac{\Omega(x,y,z)}{4\pi} D(y,z)\,dx\,dy\,dz \ , \quad (2)$$

where $\epsilon_\theta(x,y,z,\lambda_{v''k''}^{v'k'})$ and $\Omega(x,y,z)$ are the efficiency and solid angle of acceptance, respectively, of the TIF detector for photons produced at point (x,y,z) in the target cell. Thus $E_\theta(\lambda_{v''k''}^{v'k'})$ is an "effective detector efficiency" for photons (emitted in the z direction) produced by projectiles in a beam of profile $D(y,z)$.

Equation 1 is valid if (a) the radiative lifetime of the upper electronic state is sufficiently short that excited molecules decay at their points of formation in the target cell, and collisional deactivation is improbable; (b) the upper electronic state is not populated via cascade transitions from higher states, nor can it decay via other electronic transitions; and (c) the observed radiation is emitted isotropically. Conditions (a) and (b) are rather well satisfied by the excited $N_2^+(B)$ and $N_2(C)$ states,[1] the only exception being cascade population of $N_2(C)$ from $N_2(E)$. This effect and the assumption of condition (c) will be discussed in Sec. IV.

The N_{0k} in Eq. (1) were calculated from the total density N_0 of N_2 in the target cell and the relative rotational-level populations F_k by

$$N_{0k} = N_0 F_k \ . \quad (3)$$

The F_k, normalized so $\sum_k F_k = 1$, were partitioned according to a 300-K Boltzmann distribution including the statistical weights for molecular rotation and nuclear spin.

For N_2^+ $1N$ emissions, $B_{v''k''}^{v'k'}$ were evaluated with the use of a procedure described by Degen.[2] With little loss of accuracy, an approximation leading to vibrational and rotational term separability can be made, i.e.,

$$B_{v''k''}^{v'k'} \approx B_{v''}^{v'} B_{k''}^{k'} = \frac{A_{v''}^{v'}}{\sum_{v''} A_{v''}^{v'}} \frac{A_{k''}^{k'}}{\sum_{k''} A_{k''}^{k'}} \ . \quad (4)$$

The $A_{v''}^{v'}$ are defined in terms of the electronic transition moments $R_e(r_{v''}^{v'})$, where $r_{v''}^{v'}$ are the centroids for the $v' \rightarrow v''$ transitions, the Franck-Condon factors $q_{v''}^{v'}$, and the band-origin frequencies $\nu_{v''}^{v'}$ by

$$A_{v''}^{v'} = [R_e(r_{v''}^{v'})]^2 q_{v''}^{v'} (\nu_{v''}^{v'})^3 \ . \quad (5)$$

The $A_{k''}^{k'}$ are given by

$$A_{k''}^{k'} = S_{k''}^{k'} (\nu_{k''}^{k'})^3 \ , \quad (6)$$

where the $S_{k''}^{k'}$ are the rotational line strengths ($2k'$ for R-branch transitions and $2k'+2$ for P-branch transitions) and the $\nu_{k''}^{k'}$ are "reduced" rotational-line frequencies related to the actual frequencies by

$$\nu_{k''}^{k'} = \frac{\nu_{v''k''}^{v'k'}}{\nu_{v''}^{v'}} \ . \quad (7)$$

Values of $B_{v''}^{v'}$ for most of the important N_2^+ $1N$ emission bands were determined by three procedures. The first involved direct use of the $A_{v''}^{v'}$ tabulated by Degen.[2] The second used values of $q_{v''}^{v'}$, $\nu_{v''}^{v'}$, and $r_{v''}^{v'}$ from Albritton,[3] the $r_{v''}^{v'}$ being substituted into an expression for $R_e(r_{v''}^{v'})$ given by Brown and Landshoff.[4] The third used a relationship giving R_e directly as a function of $\nu_{v''}^{v'}$ from Degen,[2] the $q_{v''}^{v'}$ of Albritton,[3] and the $\nu_{v''}^{v'}$ of Gottscho *et al.*[5] whose rotational constants were also used throughout to determine $\nu_{v''k''}^{v'k'}$ and $\lambda_{v''k''}^{v'k'}$. For the N_2^+ $1N$ emission bands of interest here, the extreme differences between the $B_{v''}^{v'}$ values from the three procedures did not exceed 1.5%. Values from the third procedure are given in Table I.

The excitation cross sections were also factored into a product of electronic, vibrational, and rotational terms by the relationship

$$\sigma_{v''k''}^{v'k'} = \sigma_e P_0^{v'} P_k^{k'} \ . \quad (8)$$

Here σ_e is the total cross section for excitation of the upper electronic state, and $P_0^{v'}$ and $P_k^{k'}$ are the probabilities for the $0 \rightarrow v'$ vibrational and $k \rightarrow k'$ rotational transitions, respectively (satisfying $\sum_{v'} P_0^{v'} = \sum_{k'} P_k^{k'} = 1$).

Use of Eqs. (3), (4), and (8) allows Eq. (1) to be written as

$$\frac{S_\theta(\lambda_{v''k''}^{v'k'})}{I_b N_0} = \sigma_e P_0^{v'} B_{v''}^{v'} \left[\sum_k F_k P_k^{k'} B_{k''}^{k'} \right] E_\theta(\lambda_{v''k''}^{v'k'}) \ . \quad (9)$$

TABLE I. Branching ratios for N_2^+ $1N$ emissions for various $N_2^+(B,v') \rightarrow N_2^+(X,v'')$ vibrational transitions.

Initial B state v'	Final X state v'' 0	1	2	3	4	≥ 5
0	0.696	0.239	0.053	0.010	0.002	
1	0.360	0.238	0.267	0.103	0.026	0.006
2	0.059	0.481	0.054	0.215	0.132	0.059

Thus, the "normalized photon signal" from particular $v',k' \rightarrow v'',k''$ transitions can also be expressed as a product of electronic, vibrational, and rotational terms, and the effective detector efficiency. No further simplification of this result is generally possible, because σ_e, $P_0^{v'}$, and $P_k^{k'}$ are all dependent on the specific nature of the reaction causing the excitation. Note, however, that the product $\sigma_e P_0^{v'}$ is the cross section $\sigma_{ex}(v')$ for excitation to a particular v' level, and the product $\sigma_e P_0^{v'} B_{v''}^{v'}$ is the emission cross section $\sigma_{em}(v',v'')$ for the (v',v'') band.

However, considerable information is available for $N_2^+(B)$ formation in $e^- + N_2$ collisions. The $\sigma_{em}(v',v'')$ are known for various N_2^+ $1N$ emission bands, and the vibrational-level populations of $N_2^+(B)$ are given by the Franck-Condon factors $q_0^{v'}$ for the excitation process for e^- energies above 100 eV.[6] The $q_0^{v'}$ of Jain and Sahni[7] were used here so that $P_0^0=0.8864$, $P_0^1=0.1112$, and $P_0^2=0.002\,335$.

While the $P_k^{k'}$ are less well understood, $k \rightarrow k'$ transitions can connect only those rotational levels of equal nuclear-spin degeneracy,[8] giving the "selection rule" that $\Delta k = \pm 1, \pm 3$, etc. Furthermore, it seems physically likely that $\Delta k = \pm 1$ transitions should dominate at the relatively high e^- energy of 500 eV used here, where the excitation process should take on much of the character of photon-impact excitation. Hernandez *et al.*[9] have recently investigated how well the $\Delta k = \pm 1$ rule applies as a function of e^- energy, and reviewed the conflicting evidence of other workers. While their results suggest that some very minor violations of the $\Delta k = \pm 1$ rule may occur even at 500-eV e^- energy, the rule should be sufficiently well satisfied for use here. The $P_k^{k'}$ were thus taken to be in proportion to the rotational line strengths for photon transitions, i.e.,

$$P_k^{k'} = \begin{cases} \dfrac{(k')}{(2k'+1)}, & \text{for } k'=k+1 \\ \dfrac{(k'+1)}{(2k'+1)}, & \text{for } k'=k-1 \,. \end{cases} \tag{10}$$

With the use of the above information, the absolute photon intensity for each $v',k' \rightarrow v'',k''$ transition within the N_2^+ $1N$ emission band sequence of interest was computationally simulated for $e^- + N_2$ collisions. This simulated spectrum was then compared with that measured during TIF wavelength scans. Even though the TIF bandpass was fairly broad [with full width at half maximum (FWHM) values between 0.6 and 0.8 nm, depending on the angle of photon incidence on its surface], considerable information about $E_\theta(\lambda)$ could be obtained by summation of the computed results over the various rotational-transition wavelengths transmitted by the TIF at its various angular orientations. Additional information about $E_\theta(\lambda)$ was obtained by performing wavelength scans over atomic-line emissions resulting from e^- impact on He, Ar, and Kr atoms. Here, the normalized photon signals are directly proportional to $E_\theta(\lambda)$; for example,

$$\frac{S_\theta(\mathrm{He})}{I_b N_{\mathrm{He}}} = \sigma_{em}(\mathrm{He}) E_\theta(\lambda_{\mathrm{He}}) \,, \tag{11}$$

the proportionality constant being the appropriate emission cross section.

While $E_\theta(\lambda)$ for the H^+ and H beams were different from that for the e^- beam, the small differences could be evaluated by measurement of the beam profiles $D(y,z)$. Once $E_\theta(\lambda)$ for the H^+ and H beams had been determined, Eq. (9) could be applied to data obtained with these beams, allowing the desired $\sigma_{em}(v',v'')$ to be obtained to within the extent that estimates of $P_k^{k'}$ for $H^+ + N_2$ and $H + N_2$ collisions could be made.

The N_2 $2P$ band emissions observed from $H + N_2$ collisions were more difficult to simulate. Because these emissions result from $^3\Pi \rightarrow {}^3\Pi$ electronic transitions, each band consists of three subbands ($\sim$0.1 nm apart at their heads). Q-branch transitions and satellite-branch transitions are also present, because $N_2(C)$ and $N_2(B)$ are intermediate between Hund's coupling cases a and b (preventing definition of k' and k'').

With the use of the data of Dieke and Heath,[10] the wavelengths of the rotational transitions for the N_2 $2P$ bands of interest were computed for each subband. Because these bands are more compact than those within the N_2^+ $1N$ system (the P-, Q-, and R-branch transitions being closer together on the wavelength scale), simulated wavelength scans with the broad-bandpass TIF detector were found to be fairly insensitive to the individual rotational-transition parameters $P_k^{k'}$ and $B_{k''}^{k'}$ used for the simulations, particularly when scans over the three subbands were superimposed. Because of this, and the fact that the Q-branch and satellite-branch transitions are weak,[8] the N_2 $2P$ emission bands were approximated by three subbands with only P- and R-branch transitions present, so the same computational procedures used for the N_2^+ $1N$ simulations could be applied. Even though k' and k'' are not strictly valid quantum numbers here, it is still possible to "count" rotational levels and assign k' and k'' values[8] which should approximately describe the envelope of the rotational-line intensities observed by the TIF detector.

III. EXPERIMENTAL TECHNIQUES AND PROCEDURES

The techniques used to generate the H^+, H, and e^- particle beams and to measure the target-cell gas density have been described earlier[11,12,13] and will not be reviewed here. The particle beams were again run in 50%-duty-cycle on-off modes timed to on-off gate two pulse counters sharing the photomultiplier output for convenient separation of signal and noise. The particle-beam intensities ranged between about 10^{11} and 10^{13} particles/sec, and the N_2 target-cell pressure was typically held to well below 10^{-3} Torr (except during various diagnostic studies). These beam intensities and relative target-cell pressures were uncertain by $\pm 3\%$ and $\pm 4\%$, respectively.

The configuration of the target cell and the TIF detector is shown in Fig. 1. The viewing field of the TIF detector was established by the 1 cm by 1 cm square aperture inside the target cell and the 4-cm-diam apertures fronting lenses 1 and 2. The focal lengths of these lenses gave a $2.5\times$ demagnification of the photon-source region at the photomultiplier, the image of the emitting region thus ap-

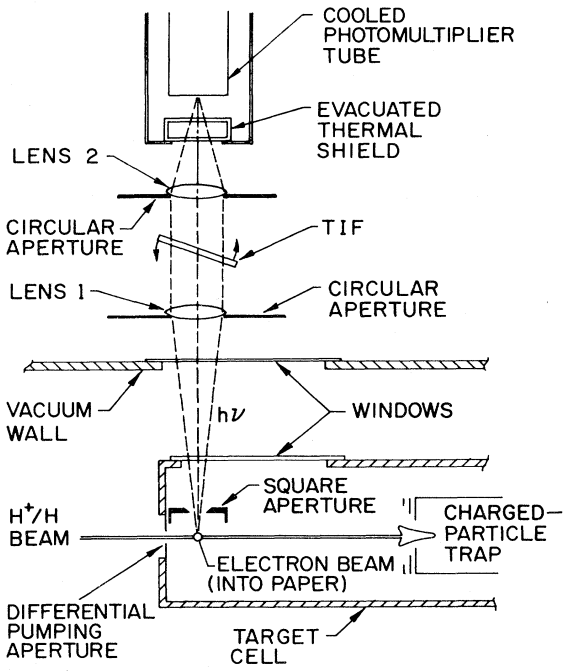

FIG. 1. Configuration of the target cell and TIF detector.

pearing as a thin strip of light about 0.4 cm long with a much smaller width of about 40% of the diameter of the projectile beams. To insure that the same portion of the photocathode received this image during e^-- as during H^+- or H-impact studies, the entire TIF detector could be turned through 90° about its optical axis (z). Thus the axis of tilt of the TIF always remained parallel to the axis (x) of the projectile beam in use (shown oriented for e^--impact studies in Fig. 1).

As noted in Sec. II, the effective detector efficiency $E_\theta(\lambda)$ was slightly different for each of the projectile beams used because of variations of the profiles $D(y,z)$ of the beams. To evaluate these relative differences via Eq. (2), these $D(y,z)$ were measured by probing the beams with thin slits which could be scanned across the extent of the beams. (The profiles typically had FWHM values less than 0.1 cm, although the H^+ beam increased to about twice this diameter at low H^+ energies.) The dependence of $\Omega(x,y,z)$ on the point of photon origin within the target cell was calculated.

Of the parameters entering the actual detector efficiency $\epsilon_\theta(x,y,z,\lambda)$, only the transmission of the TIF itself was found to have any significant dependence on the point of photon origin within the interaction region. The TIF exhibited a wavelength of maximum transmission $\lambda_f(\alpha)$ as a function of the angle α of photon incidence on its surface (relative to normal) given by

$$\lambda_f(\alpha)=\lambda_f(0)(1-K\sin^2\alpha)^{1/2}\,, \tag{12}$$

where $\lambda_f(0)$ is the wavelength of maximum transmission for normally incident photons (428.33 nm) and K is a constant (0.5061) related to the effective index of refraction of the filter. However, photons produced at points (x,y,z) in the target cell which did not lie on the z axis of the TIF detector were incident on the TIF at angles α which differed slightly from the set TIF angle θ. It was thus necessary to determine α as a function of (x,y,z) for each TIF angle θ to evaluate the relative values of $E_\theta(\lambda)$ for the projectile beams used.

As noted in Sec. II, useful information about $E_\theta(\lambda)$ for use of the 500-eV e^- beam was obtained by performing wavelength scans over atomic-line emissions from He, Ar, and Kr atoms. Figure 2 shows the result of such a scan over the spectral region containing the $6^1S\rightarrow 2^1P$ and $6^1D\rightarrow 2^1P$ transitions in He. Note that, even at the large TIF angles involved here, the transmission profile of the TIF retained its basic Gaussian shape.[14] Data such as these were used to determine values of $\lambda_f(0)$ and K appearing in Eq. (12), and to examine the dependence of the TIF's FWHM wavelength bandpass as a function of TIF angle θ. The solid curves are (normalized) computed results and illustrate how well these TIF detector properties could be fitted to such data. The peak transmission of the TIF as a function of TIF angle θ was then determined by choosing values so that the simulated wavelength scans over the N_2^+ $1N$ emission band sequence of interest for 500-eV $e^- + N_2$ collisions matched the measured wavelength-scan data for this reaction [see Fig. 4(a) in Sec. IV].

To check on how well all the properties of the TIF detector had been determined as a function of TIF angle θ, the N_2^+ $1N(0,1)$ band emission cross section was measured absolutely for 500-eV e^- impact on N_2 by a procedure using rather extreme values of θ. The N_2^+ $1N(0,1)$ photon signal measured at $\theta=4.2°$ (its maximum scan value) was compared with that resulting from e^-+He collisions at $\theta=19°$, where the $6^1S\rightarrow 2^1P$ emission signal was observed (see Fig. 2). By calculating the relative fractions of the total N_2^+ $1N(0,1)$ emission band and He line intensities that the TIF detector would observe at these respective TIF angles, the emission cross section ratio $\sigma_{em}(0,1)/\sigma_{em}(He)$ was determined. Using $\sigma_{em}(He)=3.74\times10^{-21}$ cm^2 ($\pm4.3\%$) from Van Zyl *et al.*[15] then gives $\sigma_{em}(0,1)=3.22\times10^{-18}$ cm$^2\pm10.2\%$. This cited uncertainty results from quadrature combination of all

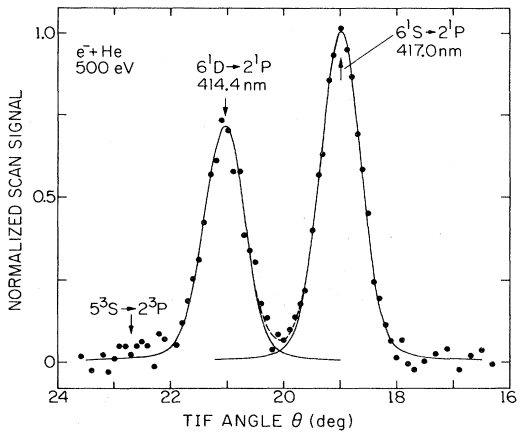

FIG. 2. Wavelength scan over atomic-line emissions produced by 500-eV e^- impact on He.

TABLE II. Measured N_2^+ $1N(0,0)$ band emission cross sections and uncertainties for 500-eV e^- impact on N_2. Units are 10^{-18} cm^2.

Workers	$\sigma_{em}(0,0)$
Aarts *et al.* (Ref. 16)	9.81±10%
Borst and Zipf (Ref. 17)	9.79±10%
Srivastava and Mirza (Ref. 18)	9.6±15%
McConkey *et al.* (Ref. 19)	9.6
Present results	9.38±10.6%

known individual uncertainties entering this measurement, including those associated with determination of $E_\theta(\lambda)$.

While other measurements of $\sigma_{em}(0,1)$ for 500-eV $e^- + N_2$ collisions are available, most workers have concentrated on measurement of $\sigma_{em}(0,0)$. These cross sections, of course, are simply related by the branching ratios B_0^0 and B_1^0. Thus, from Table I, the present "equivalent" value of $\sigma_{em}(0,0)$ is $2.912\sigma_{em}(0,1)$, or 9.38×10^{-18} cm^2, which value is compared with others in Table II. Note that all values agree to within 5%, well within mutual uncertainties, providing important supportive evidence that the properties of the TIF detector were correctly established.

To determine whether multiple collisions or other secondary effects occurring in the target cell were influencing the observed photon signals, the N_2 pressure dependence of the photon signals was studied. For N_2^+ $1N$ emissions from H^+ impact on N_2, the pressure-normalized photon signals were largely independent of N_2 pressure (although a small observed decrease in normalized photon signal with increasing N_2 pressure was properly accounted for by the use of the zero-pressure extrapolated normalized photon signals for the cross-section determinations). The normalized N_2 $2P$ photon signals from $H + N_2$ collisions were found also to have only minimal dependence on N_2 pressure. In contrast, the normalized N_2^+ $1N$ photon signals from $H + N_2$ collisions were strong functions of N_2 pressure, as illustrated in Fig. 3. Had the zero-pressure-extrapolated normalized photon signal not been used for the cross-section determination here, substantial error would have resulted.

It was tempting to attribute this normalized-photon-signal pressure dependence to secondary-e^- effects in the target cell. Secondary e^-, produced in ionizing $H + N_2$ collisions, could produce N_2^+ $1N$ emissions in "second N_2 collisions" thereby exhibiting the normalized-photon-signal pressure dependence shown in Fig. 3. Similarly, secondary e^- produced by impact of collisionally scattered H on the interior target-cell surfaces could also lead to N_2^+ emissions with this pressure dependence. (The H beam was so well aligned and small in diameter that it could not impact any surfaces during transversal of the target cell without such large-angle scattering.) However, for secondary e^- to produce N_2^+ $1N$ emissions would require secondary-e^- energies above 19 eV. Because the vast bulk of the secondary e^- produced by both of the above processes have energies below 5 eV,[20] these processes cannot explain the data in Fig. 3. (Secondary-e^- production of N_2 $2P$ emissions in the target cell should also be quite small, requiring secondary e^- with energies above 11 eV.)

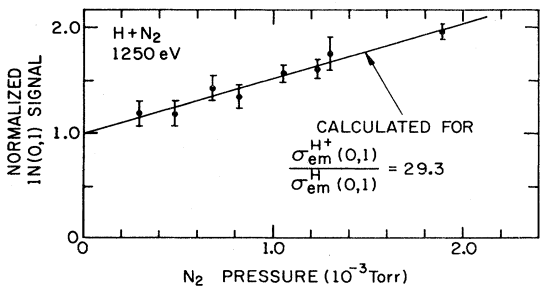

FIG. 3. N_2 pressure dependence of the normalized N_2^+ $1N(0,1)$ photon signal for studies involving H impact on N_2.

The explanation of these data lies in the fact that the N_2^+ $1N$ band emission cross sections for $H + N_2$ collisions are so much smaller than those for $H^+ + N_2$ collisions. Conversion of even a small fraction of the H entering the target cell into H^+ (via ionization-stripping reactions) prior to the photon observation region will thus result in a significant photon signal increase if the H^+ have "second collisions" within this region. Because Van Zyl *et al.*[21] have measured the ionization-stripping cross section for $H + N_2$ collisions, the fraction of the initial H converted to H^+ at the photon observation region could be calculated as a function of N_2 pressure. From this result, the data in Fig. 3 can be explained if the cross-section ratio $\sigma_{em}^{H^+}(0,1)/\sigma_{em}^{H}(0,1)=29.3$, providing a check on the relative magnitudes of these cross sections.

IV. RESULTS OF THE MEASUREMENTS

Because the TIF wavelength scans were so important to the N_2^+ $1N$ and N_2 $2P$ band emission cross-section measurements, it is useful to examine directly the four scans shown in Fig. 4. The normalized photon signals have here been set to unity near the N_2^+ $1N(0,1)$ bandhead wavelength, and a scale adjustment has been made in each case to show more detail in the N_2^+ $1N(1,2)$ and $1N(2,3)$ emission bands. The solid curves are computed results, which are discussed below.

Note how well the computed results could be fit to the measured data for $e^- + N_2$ collisions [Fig. 4(a)] by the procedures outlined in Secs. II and III. Note also how small the N_2^+ $1N(2,3)$ photon signal is for this reaction, reflecting the small value of the q_0^2 Franck-Condon factor for $N_2^+(B, v'=2)$ production.

Figures 4(b) and 4(c) show data for H^+ energies of 2 keV and 125 eV. The solid curves were computed with the use of the same rotational-excitation probabilities $P_k^{k'}$ as used for e^- impact [from Eq. (10)], but allowing for increased populations of the $v'=1$ and 2 vibrational levels of $N_2^+(B)$ relative to the $v'=0$ level. The effect of unusual vibrational excitation of these higher v' levels is quite obvious, particularly at 125-eV H^+ energy (where the decrease in resolution reflects the influence of the increased diameter of the low-energy H^+ beam on the effective detector efficiency, and the increased data scatter reflects

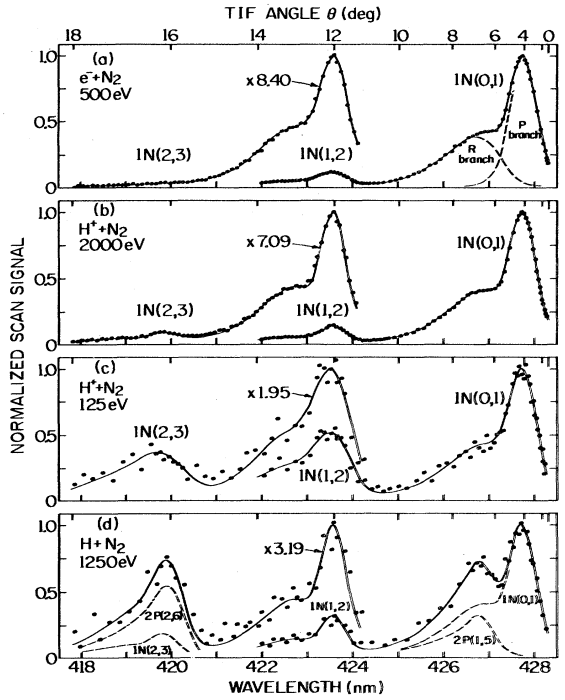

FIG. 4. Wavelength scans over the N_2^+ $1N$ and N_2 $2P$ emission bands for e^-, H^+, and H impact on N_2.

the decreased cross-section magnitudes).

As can be seen, the measured and computed scan data for the N_2^+ $1N(0,1)$ emission band for 2-keV H^+ impact are in excellent agreement and appear virtually identical to those for e^- impact. It is clear that the $P_k^{k'}$ operative in $N_2^+(B,\ v'=0)$ formation in the two processes must be reasonably similar.

However, in the far tail of the N_2^+ $1N(1,2)$ emission band (near 421 nm) for 2-keV H^+ impact, and in the far tails of all bands for 125-eV H^+ impact, the measured data lie slightly above the computed results. In these regions, where the bulk of the photon signals result from R-branch transitions from $k' \gtrsim 12$ rotational levels, there thus appears to be some evidence for the unusual rotational excitation observed by Moore and Doering.[22] In fact, if it is assumed that the rotational-level populations $F_k P_k^{k'}$ for $k' \gtrsim 12$ decrease with increasing k' in the way observed by these workers (the logarithm of the population decreasing linearly with increasing k'), the computed and measured scan data in these regions can be brought into much better agreement. This was important to properly evaluate the magnitude of (and uncertainty in) the N_2^+ $1N(2,3)$ band emission, for example, which is sensitive to "contaminating" emission from the very far tail of the N_2^+ $1N(1,2)$ band.

The wavelength-scan results for 1.25-keV H impact are shown in Fig. 4(d). As can be seen, the spectral region containing R-branch transitions from the N_2^+ $1N(0,1)$ emission band also contains substantial emission from the N_2 $2P(1,5)$ band. Fortunately, the photon signals in the vicinity of the N_2^+ $1N(0,1)$ P-branch peak are largely free of N_2 $2P(1,5)$ contamination, allowing the total measured photon signals to be computationally separated into the components shown using the simulated N_2 $2P(1,5)$ band emission spectra discussed in Sec. II.

The N_2^+ $1N(1,2)$ emission band is not subject to any appreciable N_2 $2P$ contamination. Note that, even at this fairly high H energy, the emission from this band is already significantly enhanced (about twice as much as for H^+ impact at comparable energies). The bulk of the data points in the 421-nm region also lie well above the computed curve, suggesting more unusual rotational excitation of $k' \gtrsim 12$ levels (not included in the computed curve shown) than for H^+ at similar energies.

Because the N_2^+ $1N(2,3)$ and N_2 $2P(2,6)$ emission bands are so highly overlapped, it was not possible to use the measured data to separate these photon signals. However, if it is assumed that the vibrational levels of $N_2(C)$ produced in $H + N_2$ collisions are populated according to the Franck-Condon principle for the excitation process (i.e., that $P_0^{v'} = q_0^{v'}$), a separation is possible. Taking $q_0^{v'}$ and $B_{v''}^{v'}$ values from data tabulated by Lofthus and Krupenie,[1] the N_2 $2P(2,6)$ band intensity should be about 0.61 of that for $2P(1,5)$ emission, which factor gives the N_2^+ $1N(2,3)$ and N_2 $2P(2,6)$ photon-signal separation shown in Fig. 4(d). Birely[23] has verified that $P_0^{v'} = q_0^{v'}$ for $N_2(C)$ formation in $H + N_2$ collisions for H energies down to about 2 keV, and further verification down to 150-eV H energy is provided by Bearman and Leventhal.[24] Thus, even though this assumption could not be directly verified here, it is consistent with these results and has been used for analysis of these data.[25]

The N_2^+ $1N(0,1)$, $1N(1,2)$, and $1N(2,3)$ band emission cross sections for $H^+ + N_2$ and $H + N_2$ collisions are shown in Fig. 5. The N_2^+ $1N(0,1)$ band emission cross section for $e^- + N_2$ collisions used to place these data on an absolute basis was taken to be 3.36×10^{-18} cm^2 ($\pm 10\%$), the product of the N_2^+ $1N(0,0)$ band emission cross section of Borst and Zipf[17] from Table II and the B_1^0/B_0^0 ratio of 0.343 from Table I. The $\pm 10\%$ uncertainty assigned to this cross section is the largest individual uncertainty included in the total uncertainty flags

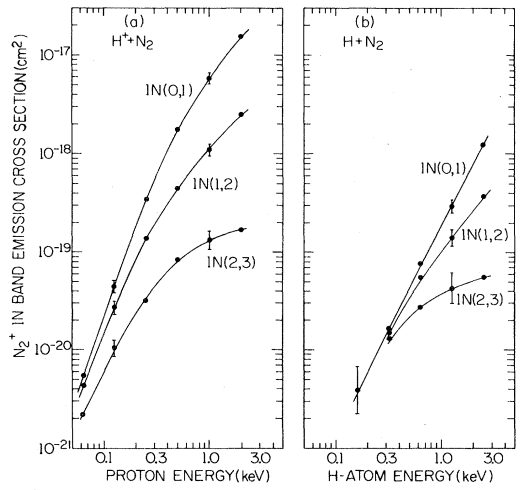

FIG. 5. N_2^+ $1N(0,1)$, $1N(1,2)$, and $1N(2,3)$ band emission cross sections for $H^+ + N_2$ and $H + N_2$ collisions.

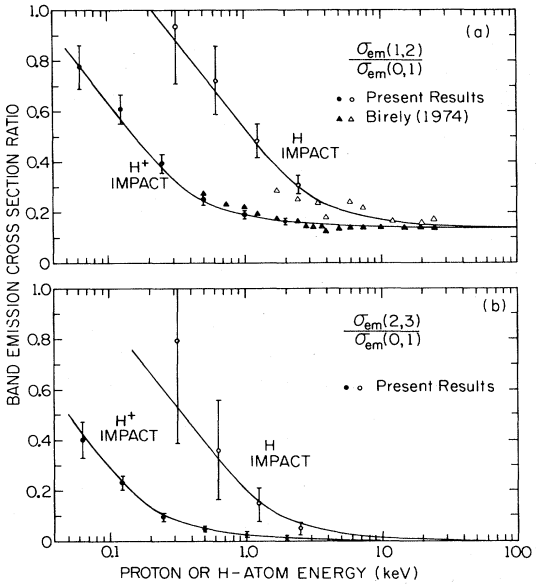

FIG. 6. N_2^+ $1N$ band emission cross-section ratios for H^+ and H impact on N_2.

shown for some of the data points in Fig. 5, which again reflect quadrature combination of all known uncertainties entering the cross-section determinations.

The only known individual uncertainty that was not evaluated here was a value of ±3.3% included to allow for the polarizations of the N_2^+ $1N$ emissions. This is equivalent to the assumption that the polarizations are less than ±10%. Because a number of workers (for example, Borst and Zipf[17] and DeHeer and Aarts[26]) have measured the polarizations of N_2^+ $1N$ emissions resulting from e^- and H^+ impact on N_2 and found values typically well below 5%, and little reason exists to believe that larger values should result from H impact, this uncertainty should be liberal.

Note that the various N_2^+ $1N$ band emission cross sections for H^+ impact are significantly larger than those for H impact. Note also that the various N_2^+ $1N$ band emission cross sections tend to approach one another in magnitude at the lower H^+ and H energies, showing the enhanced vibrational excitation of the $v'=1$ and 2 levels of $N_2^+(B)$ relative to the $v'=0$ level. This can be seen even more clearly in Fig. 6, where emission cross-section ratios are plotted. Figure 6(a) also includes the data of Birely[23] for the $\sigma_{em}(1,2)/\sigma_{em}(0,1)$ ratio which are in general agreement with the present results. While not shown, the N_2^+ $1N$ intensity ratios observed by Moore and Doering[27] for a variety of ionic projectiles impacting N_2 are also in reasonable accord with the data shown, when plotted at equivalent H^+ projectile velocities.

It is apparent that the curves drawn through the various sets of data in Fig. 6 are not necessarily the best fits to the points plotted. Rather, a "universal curve" was used, i.e., each curve has the same shape as a function of projectile energy but is displaced on the projectile-energy scale. Note that, for both emission cross section ratios, the curves for H impact lie at projectile energies a factor of 7 times as high as those for H^+ impact. The authors are not aware of any significance to be attached to this factor, or to the shape of the curve itself, other than that it reasonably fits all the measured cross-section ratios.

The cross sections $\sigma_{ex}(v')$ for excitation to the $v'=0$, 1, and 2 vibrational levels of $N_2^+(B)$ obtained from these studies are presented in Table III. These excitation cross sections were determined from $\sigma_{em}(v',v'')/B_{v''}^{v'}$ using the measured $\sigma_{em}(v',v'')$ and the $B_{v''}^{v'}$ from Table I. Also shown in Table III are values for $P_0^{v'}$ and σ_e. Because σ_e is simply $\sum_{v'}\sigma_{ex}(v')$, and only terms up to $v'=2$ could be here included in the summation, the tabulated σ_e are lower-limit values. Similarly, because $P_0^{v'}=\sigma_{ex}(v')/\sigma_e$, only upper-limit values of $P_0^{v'}$ could be determined. The tabulated $P_0^{v'}$ may be compared with $P_0^0=0.866$,

TABLE III. Cross sections for excitation to the $v'=0$, 1, and 2 vibrational levels of $N_2^+(B)$ in $H^+ + N_2$ and $H + N_2$ collisions. Units are 10^{-18} cm^2. Uncertainties are between ±10% and ±15% unless specified. Also shown are minimum values of σ_e and maximum values of $P_0^{v'}$ (see text).

H^+ energy	$v'=0$		$v'=1$		$v'=2$		
(eV)	$\sigma_{ex}(v')$	$P_0^{v'}$	$\sigma_{ex}(v')$	$P_0^{v'}$	$\sigma_{ex}(v')$	$P_0^{v'}$	σ_e
2000	63.4	<0.863	9.27	<0.126	0.785[b]	<0.011	>73.5
1000	24.1	<0.837	4.10	<0.142	0.609[a]	<0.021	>28.8
500	7.32	<0.784	1.61	<0.172	0.408[a]	<0.044	>9.34
250	1.42	<0.689	0.483[a]	<0.234	0.159[a]	<0.077	>2.06
125	0.186	<0.564	0.095[a]	<0.288	0.049[a]	<0.148	>0.330
63	0.022[a]	<0.449	0.016[b]	<0.327	0.011[b]	<0.224	>0.049
H energy							
2500	5.11	<0.743	1.37[a]	<0.199	0.398[b]	<0.058	>6.88
1250	1.21[a]	<0.626	0.511[a]	<0.265	0.210[b]	<0.109	>1.93
630	0.314[a]	<0.507	0.192[b]	<0.310	0.113[b]	<0.183	>0.619
320	0.068[b]	<0.420	0.054[b]	<0.333	0.040[b]	<0.247	>0.162
160	0.017[b]						

[a]Value uncertain by between ±15% and ±25%.
[b]Value uncertain by more than ±25%.

TABLE IV. Measured N_2 $2P(1,5)$ band emission cross section and total $N_2(C)$ production cross section for $H + N_2$ collisions. Units are 10^{-18} cm^2.

H energy (eV)	$\sigma_{em}(1,5)$	σ_e
2500	0.221(±23%)	27.6
1250	0.150(±26%)	18.7
630	0.115(±33%)	14.4
320	0.059(±34%)	7.4
160	0.027(±42%)	3.4

$P_0^1=0.111$, and $P_0^2=0.0023$, the values expected at very high projectile energies (where $P_0^{v'}=q_0^{v'}$).

While omission of $\sigma_{ex}(v')$ for $v' \geq 3$ should not seriously alter the tabulated values of σ_e and $P_0^{v'}$ at the highest projectile energies listed in Table III, the seriousness of this omission probably increases markedly with decreasing projectile energy. Using the N_2^+ $1N$ intensity ratio $I(3,4)/I(0,1) \approx 0.2$ of Moore and Doering[27] to estimate $\sigma_{ex}(v'=3)$ for an H^+ energy of 63 eV gives 0.007×10^{-18} cm^2, requiring the minimum σ_e to be increased by about 14%. The new (expanded) set of $P_0^{v'}$ becomes $P_0^0 < 0.393$, $P_0^1 < 0.286$, $P_0^2 < 0.196$, and $P_0^3 < 0.125$, the trend of which suggests that at least several higher v' levels would have to be included in any reasonably complete determination of σ_e and $P_0^{v'}$ in this low-H^+-energy region. At 320-eV H energy, the various $\sigma_{ex}(v')$ shown in Table III already have fairly similar magnitudes, suggesting that numerous higher v' levels are being populated in the $H + N_2$ collisions.

Values of the measured N_2 $2P(1,5)$ band emission cross section for $H + N_2$ collisions are given in Table IV with their uncertainties (including a value of ±6.7% to account for the unknown emission polarization). Concern also exists here about cascade population of $N_2(C)$ from the metastable $N_2(E)$. However, both Birely[23] for $H + N_2$ collisions and Freund[28] for $e^- + N_2$ collisions suggest that the 0th vibrational level of $N_2(E)$ is dominantly populated in such collisions, and Freund[28] also reports that decay of $N_2(E)$ to $N_2(C)$ "proceeds almost exclusively" via (0,0) vibrational transitions. Thus the cascade population of $N_2(C, v'=1)$ should be even smaller than the "few percent" cascade population of $N_2(C, v'=0)$ noted by Birely,[23] and has thus been ignored. Similarly, cascade population of $N_2(C, v'=2)$ should not be significant and, as noted earlier, the N_2 $2P(2,6)$ band emission cross section should be about 0.61 times that for $2P(1,5)$ band emission.

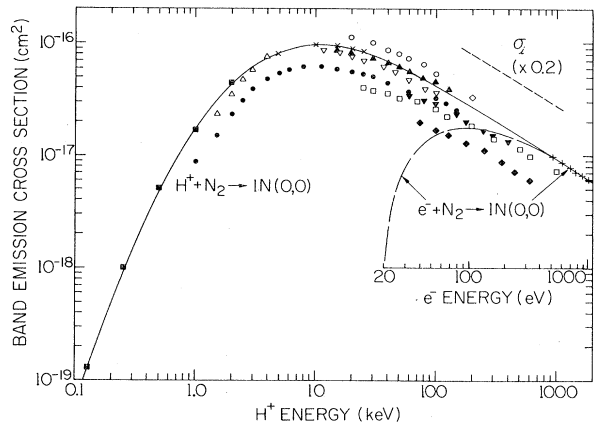

FIG. 7. Cross sections for N_2^+ $1N(0,0)$ band emission for $H^+ + N_2$ collisions. Data are as follows: ■, present results; △, Carleton and Lawrence (Ref. 29); ●, DeHeer and Aarts (Ref. 26); ×, Sheridan *et al.* (Ref. 30); ▽, Hoffman *et al.* (Ref. 31); ○, Gardiner *et al.* (Ref. 32); ▲, Philpot and Hughes (Ref. 33); □, Dufay *et al.* (Ref. 34); ▼, Robinson and Gilbody (Ref. 35); ◇, Hughes *et al.* (Ref. 36); and ◆, Thomas *et al.* (Ref. 37). Some data have been adjusted (see text). e^--impact data are from Borst and Zipf (Ref. 17). Short-dashed curve is 0.2 times the cross section σ_i for total ionization of N_2 by H^+ impact from McDaniel *et al.* (Ref. 38).

Values of the total cross section σ_e for $N_2(C)$ production in $H + N_2$ collisions, determined by assuming that no unusual vibrational excitation occurs in the excitation process, are also given in Table IV. These results were obtained from $\sigma_e = \sigma_{em}(v',v'')/P_0^{v'}B_{v''}^{v'}$ using the measured N_2 $2P(1,5)$ band emission cross section and $P_0^1=q_0^1=0.305$ and $B_5^1=0.0262$ from Lofthus and Krupenie.[1]

V. COMPARISONS WITH OTHER DATA

Because most investigations of N_2^+ $1N$ emissions from $H^+ + N_2$ and $H + N_2$ collisions have concentrated on measurement of the N_2^+ $1N(0,0)$ band emission cross section, the comparisons here will be made on this basis. The present results for $\sigma_{em}(0,0)$ were obtained from $\sigma_{em}(0,0)=2.912\sigma_{em}(0,1)$, using the branching ratios in Table I and the measured N_2^+ $1N(0,1)$ band emission cross section.

Figure 7 shows the results of a number of $\sigma_{em}(0,0)$ measurements for $H^+ + N_2$ collisions. Not all available data are represented here, but an attempt was made to include most results which were placed on an absolute basis by calibration of the photon detectors used by procedures which did not involve simply normalizing the data to other measurements of the same cross section. The results of Sheridan *et al.*[30] have been plotted at magnitudes of 1.60 times their published values for reasons discussed below. Also shown is the N_2^+ $1N(0,0)$ band emission cross section of Borst and Zipf[17] for $e^- + N_2$ collisions, plotted at the same e^- and H^+ velocities, and the total cross section σ_i for ionization of N_2 by H^+ impact from McDaniel *et al.*[38] As can be seen, the various $\sigma_{em}(0,0)$ measurements show very similar H^+ energy dependences, but exhibit a wide range of cross-section magnitudes.

At very high H^+ energies (~1000 keV), the N_2^+ $1N(0,0)$ band emission cross section should result almost entirely from the $H^+ + N_2 \rightarrow H^+ + N_2^+(B) + e^-$ ionization reaction, as opposed to the $H^+ + N_2 \rightarrow H + N_2^+(B)$ electron-capture reaction known to dominate at lower H^+ energies.[39,40] Thus, in this high-H^+-energy region, $\sigma_{em}(0,0)$ for H^+ and e^- impact on N_2 should be the same when compared at identical projectile velocities (the ionization process being independent of the sign of the charge of these projectiles). Borst and Zipf[17] also report that for e^- energies above a few hundred eV, the N_2^+ $1N(0,0)$ band emission cross section is about 7% as large as the total cross section for ionization of N_2 by e^- impact. This

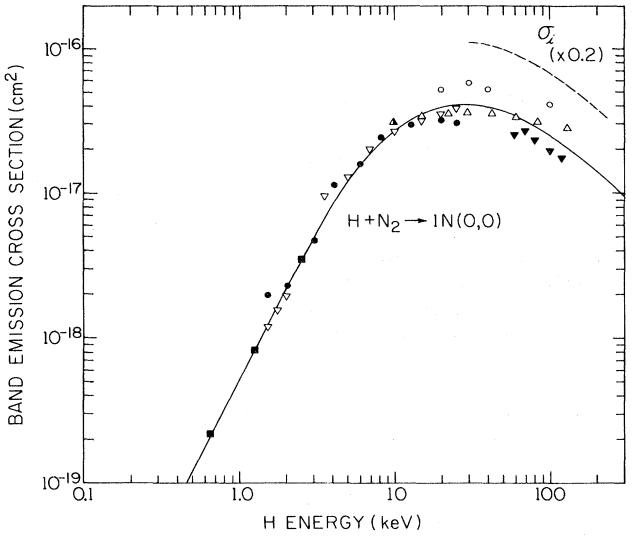

FIG. 8. Cross sections for N_2^+ $1N(0,0)$ band emission for $H + N_2$ collisions. Data are as follows: ■, present results; ●, Birely (Ref. 23), ▽, McNeal and Clark (Ref. 41); ○, Gardiner *et al.* (Ref. 32); ▼, Robinson and Gilbody (Ref. 35); and △, Dahlberg *et al.* (Ref. 42). Some data have been adjusted (see text). Dashed curve is 0.2 times the cross section σ_i for total ionization of N_2 by H impact from Solov'ev *et al.* (Ref. 43).

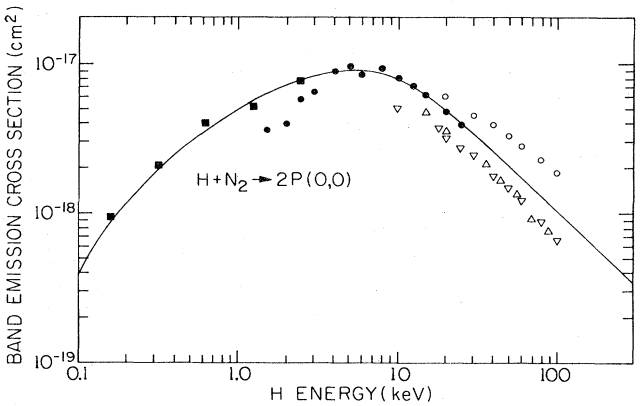

FIG. 9. Cross sections for N_2 $2P(0,0)$ band emission for $H + N_2$ collisions. Data are as follows: ■, present results; ●, Birely (Ref. 23); ○, Gardiner *et al.* (Ref. 32); ▽, Hoffman *et al.* (Ref. 44); and △, Dahlberg *et al.* (Ref. 42). Some data have been adjusted (see text).

value is the same as the $\sigma_{em}(0,0)/\sigma_i$ ratio obtained from the data in Fig. 7 for $H^+ + N_2$ collisions, providing supportive evidence for the similarity of these reaction processes.

Because the $\sigma_{em}(0,0)$ of Borst and Zipf[17] for $e^- + N_2$ collisions was employed as the calibration standard for the N_2^+ $1N$ band emission cross-section measurements for $H^+ + N_2$ collisions reported here, the data in Fig. 7 for very high and very low H^+ energies share the same absolute normalization. Furthermore, Sheridan *et al.*[30] also compared directly the $\sigma_{em}(0,0)$ for e^- and H^+ impact on N_2. While, in the opinion of the present authors, their procedures for absolute calibration of the photon detector used were not highly accurate, the relative values of their $\sigma_{em}(0,0)$ should be accurate. Thus the multiplicative factor of 1.6 needed to bring their $\sigma_{em}(0,0)$ for 500-eV e^- impact on N_2 into agreement with that obtained by Borst and Zipf[17] was also applied to their $\sigma_{em}(0,0)$ for $H^+ + N_2$ collisions. Therefore, the line curve through their adjusted data points and the present low-H^+-energy results in Fig. 7 can be traced directly to the $e^- + N_2$ studies of Borst and Zipf.[17]

Figure 8 shows that far fewer measurements of $\sigma_{em}(0,0)$ for $H + N_2$ collisions are available. In fact, of the results plotted, only the present data, those of Robinson and Gilbody,[35] and those of Gardiner *et al.*[32] represent absolute measurements. However, Birely,[23] McNeal and Clark,[41] and Dahlberg *et al.*[42] all measured relative $\sigma_{em}(0,0)$ values for H and H^+ impact on N_2. These respective results for $H + N_2$ collisions were therefore placed on (new) absolute scales by normalization of their H^+-impact data to the line curve in Fig. 7.

As can be seen, this normalization brings all the $\sigma_{em}(0,0)$ data into fair accord. Note that the results of Robinson and Gilbody[35] and of Gardiner *et al.*[32] lie about as far below and above the line curve, respectively, as the results of these same workers do for $H^+ + N_2$ collisions (suggesting that photon-detector-calibration differences are likely responsible for these discrepancies). Note also that once again, the plotted $\sigma_{em}(0,0)$ cross-section curve is about 7% as large as the total cross section for ionization of N_2 by H impact[43] at the higher H energies.

Values of the N_2 $2P(0,0)$ band emission cross section from a variety of sources for $H + N_2$ collisions are plotted in Fig. 9. Of the results cited, only those of Hoffman *et al.*[44] have been plotted as reported. The relative measurements of Birely[23] and of Dahlberg *et al.*[42] have again been scaled by the same factors used to adjust their N_2^+ $1N(0,0)$ band emission cross sections for $H + N_2$ collisions discussed above. The present results and those of Gardiner *et al.*[32] have been computed from N_2 $2P(1,5)$ and $2P(0,2)$ band emission cross-section measurements, respectively, using the appropriate branching ratios[1] and the assumption that no unusual vibrational excitation occurs in $N_2(C)$ formation in $H + N_2$ collisions: thus $\sigma_{em}(0,0) = 34.7\sigma_{em}(1,5) = 4.16\sigma_{em}(0,2)$. Note that again, the data of Gardiner *et al.*[32] lie above the curve drawn in Fig. 9, and that the results of Hoffman *et al.*[44] lie about as much below the curve as their N_2^+ $1N(0,0)$ band emission cross-section values[31] do for $H^+ + N_2$ collisions, the consistency of which is pleasing.

In a very real sense, the $\sigma_{em}(0,0)$ cross-section curves drawn in Figs. 7, 8, and 9 can thus be traced to the N_2^+ $1N(0,0)$ band emission cross-section measurements of Borst and Zipf[17] for $e^- + N_2$ collisions. If this cross section should be found to be in error, the results presented here could be adjusted accordingly. However, the good agreement of the $\sigma_{em}(0,0)$ values presented in Table II for $e^- + N_2$ collisions appears to make this prospect unlikely.

ACKNOWLEDGMENTS

The authors express their thanks to R. C. Amme for his contribution to this research. This work has been supported by the Aeronomy Program, Division of Atmospheric Sciences, National Science Foundation.

[1]A. Lofthus and P. H. Krupenie, J. Phys. Chem. Ref. Data 6, 113 (1977).
[2]V. Degen, J. Quant. Spectrosc. Radiat. Transfer 18, 113 (1977).
[3]D. L. Albritton (private communication).
[4]W. A. Brown and R. K. Landshoff, J. Quant. Spectrosc. Radiat. Transfer 11, 1143 (1971).
[5]R. A. Gottscho, R. W. Field, K. A. Dick, and W. Benesch, J. Mol. Spectrosc. 74, 435 (1979).
[6]J. P. Doering, in *Abstracts of Papers, Seventh International Conference on the Physics of Electronic and Atomic Collisions, Amsterdam, 1971* (North-Holland, Amsterdam, 1972), p. 341.
[7]D. C. Jain and R. C. Sahni, Int. J. Quantum Chem. 2, 325 (1968).
[8]G. Herzberg, *Spectra of Diatomic Molecules* (Van Nostrand, New York, 1950).
[9]S. P. Hernandez, P. J. Dagdigian, and J. P. Doering, J. Chem. Phys. 77, 6021 (1982).
[10]G. H. Dieke and D. F. Heath, Johns Hopkins Spectroscopy Report No. 17, Department of Physics, Johns Hopkins University, 1959 (unpublished).
[11]B. Van Zyl, N. G. Utterback, and R. C. Amme, Rev. Sci. Instrum. 47, 814 (1976).
[12]B. Van Zyl, H. Neumann, H. L. Rothwell, Jr., and R. C. Amme, Phys. Rev. A 21, 716 (1980).
[13]B. Van Zyl, H. L. Rothwell, Jr., and H. Neumann, Phys. Rev. A 21, 730 (1980).
[14]This TIF maintained its basic Gaussian transmission profile up to TIF angles of about 25°. However, a second TIF from the same manufacturer exhibited an increasingly non-Gaussian transmission profile for TIF angles above 8°. Such filters must be individually characterized when used in this way.
[15]B. Van Zyl, G. H. Dunn, G. Chamberlain, and D. W. O. Heddle, Phys. Rev. A 22, 1916 (1980).
[16]J. F. M. Aarts, F. J. DeHeer, and D. A. Vroom, Physica 40, 197 (1968).
[17]W. L. Borst and E. C. Zipf, Phys. Rev. A 1, 834 (1970).
[18]B. N. Strivastava and I. M. Mirza, Phys. Rev. 176, 137 (1968).
[19]J. W. McConkey, J. M. Woolsey, and D. J. Burns, Planet. Space Sci. 15, 1332 (1967).
[20]While no detailed e^--energy distributions are available for secondary e^- produced in low-energy H + N_2 or H + surface collisions, both processes have been studied in the authors' laboratory. In addition to Ref. 21 below, see B. Van Zyl, T. Q. Le, H. Neumann, and R. C. Amme, Phys. Rev. A 15, 1871 (1977); J. A. Ray, C. F. Barnett, and B. Van Zyl, J. Appl. Phys. 50, 6516 (1979). From the collection fields required to gather secondary e^- from these processes, it was established that few of the secondary e^- could have energies much in excess of 5 eV.
[21]B. Van Zyl, H. Neumann, T. Q. Le, and R. C. Amme, Phys. Rev. A 18, 506 (1978).
[22]J. H. Moore and J. P. Doering, Phys. Rev. 182, 176 (1969).
[23]J. H. Birely, Phys. Rev. A 10, 550 (1974).
[24]G. H. Bearman and J. J. Leventhal, Phys. Rev. A 17, 80 (1978).
[25]At the lowest H energies, where the N_2 $2P(1,5)$ and $2P(2,6)$ band emission photon signals dominated the wavelength-scan data for H + N_2 collisions, it was possible to at least approximately verify this assumption here. However, the data were sufficiently scattered that the conclusion $0.40 < \sigma_{em}(2,6)/\sigma_{em}(1,5) < 0.80$ was not highly definitive.
[26]F. J. DeHeer and J. F. M. Aarts, Physica 48, 620 (1970).
[27]J. H. Moore and J. P. Doering, Phys. Rev. 177, 218 (1969).
[28]R. S. Freund, J. Chem. Phys. 50, 3734 (1969).
[29]N. P. Carleton and T. R. Lawrence, Phys. Rev. 109, 1159 (1958).
[30]W. F. Sheridan, O. Oldenberg, and N. P. Carleton, J. Geophys. Res. 76, 2429 (1969).
[31]J. M. Hoffman, G. J. Lockwood, and G. H. Miller, Phys. Rev. A 11, 841 (1975).
[32]H. A. B. Gardiner, W. R. Pendleton, Jr., J. J. Merrill, and D. J. Baker, Phys. Rev. 188, 257 (1969).
[33]J. L. Philpot and R. H. Hughes, Phys. Rev. 133, A107 (1964).
[34]M. Dufay, J. Desesquelles, M. Druetta, and M. Eidelsberg, Ann. Geophys. 22, 614 (1966).
[35]J. M. Robinson and H. B. Gilbody, Proc. Phys. Soc. London 76, 589 (1967).
[36]R. H. Hughes, J. L. Philpot, and C. Y. Fan, Phys. Rev. 123, 2084 (1961).
[37]E. W. Thomas, G. D. Bent, and J. L. Edwards, Phys. Rev. 165, 32 (1968).
[38]E. W. McDaniel, J. W. Hooper, D. W. Martin, and D. S. Harmer, in *Abstracts of Papers, Fifth International Conference on Ionization Phenomena in Gases* (North-Holland, Amsterdam, 1962), p. 60.
[39]P. J. Wehrenberg and K. C. Clark, Phys. Rev. A 8, 173 (1973).
[40]J. M. Hoffman, G. J. Lockwood, and G. H. Miller, Phys. Rev. A 23, 2983 (1981).
[41]R. J. McNeal and D. C. Clark, J. Geophys. Res. 74, 5065 (1969).
[42]D. A. Dahlberg, D. K. Anderson, and I. E. Dayton, Phys. Rev. 164, 20 (1967).
[43]E. S. Solov'ev, R. N. Il'in, V. A. Oparin, and N. V. Fedorenko, Zh. Eksp. Teor. Fiz. 42, 659 (1962) [Sov. Phys.—JETP 15, 459 (1962)].
[44]J. M. Hoffman, G. J. Lockwood, and G. H. Miller, Phys. Rev. A 7, 118 (1973).